19th Brazilian Congress of Thermal Sciences and Engineering
November 6th–10th, 2022, Bento Gonçalves - RS - Brazil

ENC-2022-0245
DISPLACEMENT EFFICIENCY IN WASHOUT ZONES DURING WELL CONSTRUCTION

Priscilla Ribeiro Varges
Bruno da Silva Fonseca
Lorena C. Moraes
Elias C. Rodrigues
Mônica Feijó Naccache
Paulo Roberto de Souza Mendes
Department of Mechanical Engineering, Pontifícia Universidade Católica do Rio de Janeiro, Rua Marquês de São Vicente 225, Rio de Janeiro, RJ 22453-900, Brazil
prvarges@puc-rio.br, fonseca_bruno@puc-rio.br, lorenarcmoraes@gmail.com, ecr@esp.puc-rio.br, naccache@puc-rio.br, pmendes@puc-rio.br

Carlos Pessanha Costa Carvalho
André Leibsohn Martins
Ingrid Ezechiello da Silva
Cenpes/Petrobras, R. Horácio Macedo, 950, Ilha do Fundão, Rio de Janeiro - RJ, CEP 21941-915
carlos.pessanha@petrobras.com.br, aleibsohn@petrobras.com.br, iezechiello@petrobras.com.br

Pedro J. Tobar Espinoza
Universidad Ecotec, Km 13.5 Via Samborondón, Samborondón, Guayas, Ecuador
ptobare@ecotec.edu.ec

Abstract. *In the oil industry, drilling, cementing and well completion operations involve the flow, replacement and displacement of fluids. Especially, structured fluids such as cement slurries, drilling fluids, viscous pills and other suspensions and emulsions, which mechanical behavior are typically elasto-viscoplastic, are part of the process. To ensure the success and optimization of such operations, the displacement flows must be accurately predicted. An unsuccessful operation can compromise the well's safety and integrity through undesired inflow into the well, wellbore collapse, inefficient cuttings transport, failure to isolate zones during cementing, among others. A challenging situation occurs when fluids with different densities flow in enlarged zones (washout). This work provides a comprehensive analysis of the displacement process of Newtonian and non-Newtonian fluids through concentric and vertical annular expansions-contractions as a function of rheology, density ratio, flow rate and geometry. The problem was numerically and experimentally analyzed in order to explore the influence of the governing parameters on displacement efficiency. Results showed that hydrodynamic instabilities can appear in a variety of situations. The finite volume method was used to solve the governing mass and momentum conservation equations. To solve the multiphase problem, the volume of fluid method was used. Furthermore, experiments were performed with Carbopol aqueous dispersion been displaced by a glycerin/water mixture varying the dimensions of the geometry and the injection flow rate. A Coriolis flowmeter was used to measure the flow rate and the density of the fluids leaving the test section in order to determine the displacement efficiency. Excellent agreement was observed between numerical and experimental results. It was observed that density ratio plays a major role on displacement efficiency and that the diameter of the eroded zones has a significant impact on the amount of fluid retained inside the cavity. Ultimately, numerical simulations were performed considering geometric dimensions, fluids properties and flow rates typical of oil well cementing operations.*

Keywords: *Liquid-liquid displacement, Cementing operation, Washout, Viscoplastic materials*

1. INTRODUCTION

The cementation process of oil wells is one of the most important processes in the oil industry and it is directly related to the well lifetime (Naccache *et al.*, 2018). Primary cementing is a technique used to place cement slurries into the annular space after the casings are lowered into the well. The main purposes of this operation are to provide mechanical support

and to provide hydraulic seal preventing fluids influx from the formation (Frigaard *et al.*, 2017).

This process involves drilling fluids and cement slurries, both yield stress materials. Ideally, the drilling fluid must be completely removed from the borehole and a complete filling of the cross section with the cement slurry must occur (Varges *et al.*, 2020). Moreover, displacement of yield stress fluids presents several challenges, which includes static fluid layers (Moyers-Gonzalez and Frigaard, 2008), unyielded regions (Denn and Bonn, 2010) and viscous fingering instabilities (Lindner *et al.*, 2000).

The wellbore surface may present irregularities caused by erosion or a poorly consolidated formation (Espinoza *et al.*, 2022), which makes more difficult to predict flow displacement efficiency. Roustaei *et al.* (2015) observed that the area of the yielded region is not affected by the erosion geometry when considering a material with high yield stress and a geometry with a deep erosion. Furthermore, Naccache *et al.* (2018) numerically explored the displacement efficiency of yield stress materials through a model eroded well. It was noted that inertia breaks the fore-aft symmetry of the interface between the fluids.

Regarding the effect of increasing Reynolds number (Re) in the removal volume of an eroded region, an interesting result was observed by Espinoza *et al.* (2022). They found an inversely proportional relation between Reynolds number and removed volume from an eroded region. A similar result was also pointed out by Etrati *et al.* (2020) wherein shows that at large enough Re the flow destabilizes within the eroded zone, recirculates and mixes with the displacing fluid, this process may or may not improve the actual displacement.

The goal of this work is to better understand the displacement flow of complex fluids in an eroded borehole in order to optimize cementing operations in the oil industry. The influence of geometric, rheological and flow parameters are experimentally and numerically investigated in the displacement efficiency.

2. PHYSICAL MODEL

The flow geometry, an annular vertical abrupt expansion–contraction used to model the eroded borehole with column, is presented in Figure 1. The upstream and downstream length, and the diameter of the outer tube are equal to l and d, respectively, while the inner tube diameter is defined as d'. The cavity axial length and diameter are L and D, respectively.

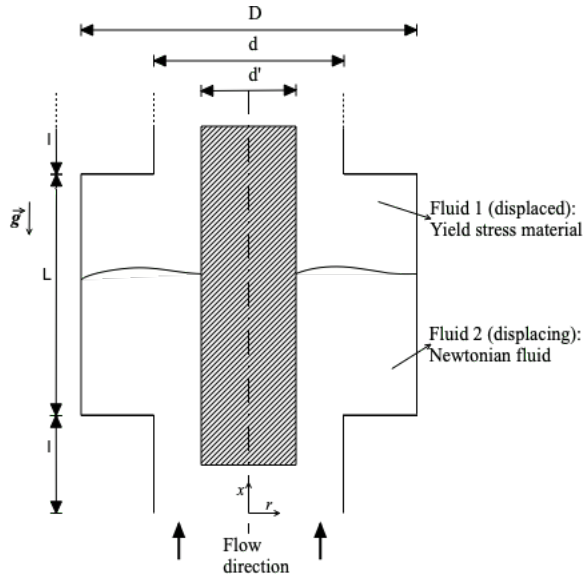

Figure 1. Schematic of the annular abrupt expansion-contraction geometry.

The upstream and downstream tubes length were kept equal to $l = 5D_h$ to avoid any disturbances inside the enlargement region due to entrance and exit boundaries. The hydraulic diameter is defined as $D_h = d - d'$. Well eccentricity and inclination were not explored.

The scaling was discussed in (Espinoza *et al.*, 2022), where the dimensionless geometry parameters are: $D^* = D/d$, which is called cavity diameter, $L^* = L/d$ is the cavity length, $d'^* = d'/d$ is the inner tube diameter, and $l^* = l/d$ is the inner and outer tube length. Moreover, the density difference is defined as $\rho^* = (\rho_2 - \rho_1)/\rho_2$ and the viscosity ratio is $\eta^* = \mu_2/\eta_{1,c}$, being $\eta_{1,c}$ the characteristic viscosity given by $\eta_c = \eta(\dot{\gamma}_c)$ obtained at a characteristic shear rate $\dot{\gamma}_c = V/D_h$. Ultimately, the Reynolds number is defined as the maximum value at the annular space. Then, $Re =$

$max(4\rho_1 Q D_h/(\pi(d^2-d'^2)\eta_{1,c}), 4\rho_2 Q D_h/(\pi(d^2-d'^2)\mu_2))$.

3. NUMERICAL PROCEDURE

Two-dimensional numerical solutions were obtained using Ansys®Fluent (Ansys Inc.) considering laminar, axisymmetric, isothermal, and isochoric flows.

The governing equations are:

$$\nabla \cdot \boldsymbol{v} = 0 \tag{1}$$

$$\rho\left[\frac{\partial \boldsymbol{v}}{\partial t} + \boldsymbol{v}\cdot\nabla\boldsymbol{v}\right] = -\nabla p + \nabla\cdot\boldsymbol{\sigma} + \rho\boldsymbol{g} \tag{2}$$

where $\boldsymbol{v}$ is the velocity field; p is the pressure field; ρ is the mixture density; and $\boldsymbol{g}$ is the acceleration due to gravity. The quantity $\boldsymbol{\sigma}$ is the extra-stress tensor, assumed to obey the generalized Newtonian fluid model, namely $\boldsymbol{\sigma} = \eta(\dot{\gamma})\dot{\boldsymbol{\gamma}}$, where $\dot{\boldsymbol{\gamma}} \equiv [\nabla\boldsymbol{v} + \nabla\boldsymbol{v}^T]$ is the rate of strain tensor.

The fluids are assumed to be immiscible and incompressible. The displacing fluid, fluid 2, is Newtonian, so the viscosity is constant and equal to μ_2. The displaced fluid, fluid 1, is a yield stress material, modeled by the following regularized Herschel-Bulkley viscosity function (ANSYS, 2020):

$$\eta(\dot{\gamma}) = \begin{cases} \dfrac{\sigma_y}{\dot{\gamma}} + K(\dot{\gamma})^{n-1} & \text{if } \dot{\gamma} \geq \dot{\gamma}_{cr} \\ \dfrac{\sigma_y}{\dot{\gamma}_{cr}}\left[2 - \dfrac{\dot{\gamma}}{\dot{\gamma}_{cr}}\right] + K\dot{\gamma}_{cr}^{n-1}\left[(2-n) + (n-1)\dfrac{\dot{\gamma}}{\dot{\gamma}_{cr}}\right] & \text{if } \dot{\gamma} < \dot{\gamma}_{cr} \end{cases} \tag{3}$$

where $\dot{\gamma} \equiv \sqrt{\frac{1}{2}\mathrm{tr}\dot{\boldsymbol{\gamma}}^2}$ is the intensity of the rate of strain, σ_y is the yield stress, K is the consistency index, n is the power-law index and $\dot{\gamma}_{cr}$ is the regularization parameter, given by the small rate-of-strain below which the viscosity is equal to a constant high value $\approx 500\eta_c$ (Burgos and Alexandrou, 1999; Soares *et al.*, 2003; Beverly and Tanner, 1992). Then $\dot{\gamma}_{cr} \approx \sigma_y/500\eta_c$.

To handle the two fluid phases, the Eulerian Volume of Fluid Method (VoF) was employed. The volume fractions ϕ_i ($i = 1, 2$) are obtained by solving the mass conservation equation, Eq. (4) for one of the phases along with the constraint equation, Eq. (5):

$$\frac{\partial \phi_i}{\partial t} + \boldsymbol{v}\cdot\nabla\phi_i = 0, \quad i = 1 \text{ or } 2 \tag{4}$$

$$\sum_{i=1}^{2}\phi_i = 1 \tag{5}$$

The initial and boundary conditions used in the simulations were such as to represent the cementing operation. The no-slip and impermeability conditions were assumed at all walls. Initially the whole domain is filled with fluid 1 and the velocity is zero. At the instant $t = 0$, Fluid 2 is injected with a developed (parabolic) flow profile with average velocity V. The flow is assumed fully developed at outlet. Interfacial tension was not considered.

The finite volume method is used to discretize the conservation equations. To numerically solve the governing equations, a first order implicit-transient-formulation pressure-based solver was used, including the PRESTO! (PREssure Staggering Option) discretization scheme for pressure, the second-order upwind for momentum, least squares cell-based for the gradient, the geo-reconstruct algorithm for the volume fraction and the PISO algorithm for the pressure-velocity coupling (ANSYS, 2020). The simulations were carried out up to the time instant where one test section volume had been injected. A non-uniform mesh with 348,824 nodes was generated with GMSH software, and chosen after some mesh tests were performed.

4. EXPERIMENTS

Experiments to study the displacement of a non-Newtonian fluid by a Newtonian fluid were carried out for different configurations. The displacer fluid, which is denser, was represented by an aqueous solution of glycerin and the displaced fluids are different aqueous solutions of Carbopol.

Figure 2 present the experimental setup. Three fluid reservoirs are connected to a double-headed peristaltic pump with a pulse damper through valves and silicone hoses. The test section, which is on the other side of the pump, consist of an annular geometry whose external wall possessed a sudden expansion–contraction, as can be seen in Fig. 3. A Coriolis flowmeter was positioned at the outlet of the test section, to measure the flow rate and density of the fluids leaving the test section.

Figure 2. Experimental setup.

Figure 3. Test section.

It is interesting to note that all cases present low Re, which means that we only investigated laminar flows. Furthermore, all cases present $\eta^* < 1$, indicating the occurrence of unstable flows leading to viscous fingering formation thus reducing the displacement efficiency. It should be noted that η^* is defined at a critical shear rate at the inlet annulus so it does not represent a fixed and constant value throughout the entire geometry. Therefore, locally there are regions with different values of η^*.

The displacement efficiency Φ is defined as the ratio of the displaced volume to the total volume.

$$\Phi = \frac{V_{displaced}}{V_{Total}} \tag{6}$$

In the experimental case, the displacement efficiency is calculated in relation to the entire geometry because, due to experimental limitations, it is not possible to separate the contribution of the cavity from the annulus to the calculation of the efficiency. In the numerical case, the displacement efficiency is calculated only in the cavity as it is our region of interest.

5. RESULTS

5.1 EXPERIMENTAL RESULTS

Comparisons were made between experiments and numerical simulations in order to validate the numerical methodology implemented. More results are found in (Espinoza *et al.*, 2022; Varges *et al.*, 2022; Espinoza, 2020).

Figure 4 present, as an example, the displacement efficiency as a function of time considering $\rho^* = 0.187$, $d'^* = 0.846$, $D^* = 4.25$, $L^* = 2.70$, $\eta^* = 0.016$ and $Re = 8.28$, which represents a 0.1% Carbopol aqueous dispersion ($\tau_y = 2.96\,Pa$, $k = 1.35\,Pa.s^n$ and $n = 0.47$) been displaced by glycerin/water mixture ($\mu = 0.032\,Pa.s$). Diffusion effects are negligible, as can be seen in Espinoza (2020). Moreover, Figure 5 presents the time evolution (from left to right) of fluid interface at plane rz. It can be observed a good agreement between the experimental and numerical data.

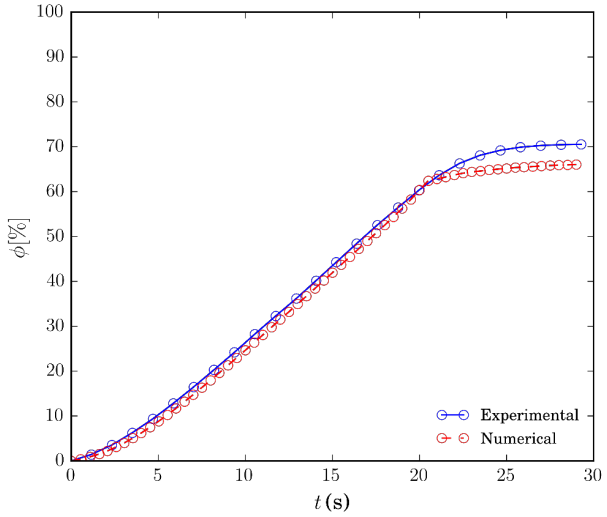

Figure 4. Displacement efficiency as a function of time for $\rho^* = 0.187$, $d'^* = 0.846$, $D^* = 4.25$, $L^* = 2.70$, $\eta^* = 0.016$ and $Re = 8.28$.

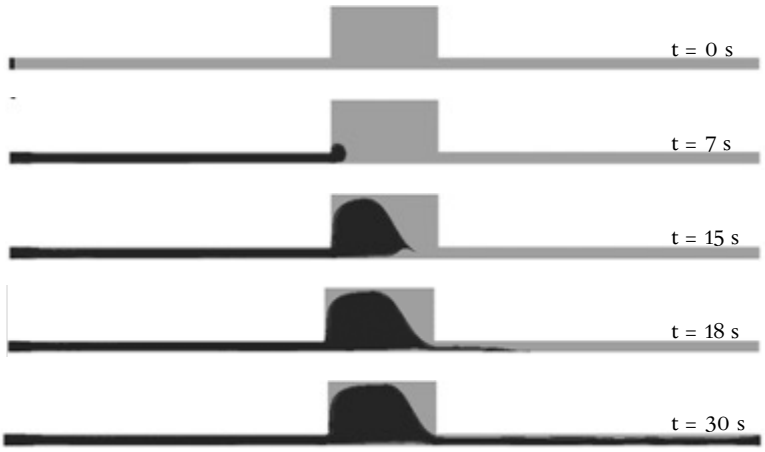

Figure 5. Time evolution for $\rho^* = 0.187$, $d'^* = 0.846$, $D^* = 4.25$, $L^* = 2.70$, $\eta^* = 0.016$ and $Re = 8.28$. The Newtonian displacing fluid is represented in black, and the displaced viscoplastic material in gray.

5.2 NUMERICAL RESULTS

The results of flow displacement were obtained for different combinations of flow parameters, fluids rheology and geometry. Tables 1 and 2 present the non-Newtonian and Newtonian fluids properties at 25°C, which were obtained according R. Varges *et al.* (2019). Flow rates of 4 and 15 bpm were explored leading to inertia flows since $4 < Re < 1800$ and to a range of $0.0038 < \eta^* < 11.64$.

Figure 6 presents data from 24 combinations of parameters that were evaluated in numerical simulations considering the inlet and outlet annulus length of 0.33m, the well diameter of 12.25" and the casing diameter is 9.625". In general terms,

Table 1. Non-Newtonian fluids properties.

$\tau_{y,1}$ $[lbf/100ft^2]$	K $[lbf.s^n/100ft^2]$	n [ ]	ρ_1 $[lb/gal]$
3.57	0.11	0.78	10.00
25.06	3.39	0.34	16.50
19.30	16.00	0.30	16.50

Table 2. Newtonian fluids properties.

μ_2 $[cP]$	ρ_2 $[lb/gal]$
7	9.9
7000	9.9
120	9.9
40	9.9
12161	16.0
111	16.0
88	16.0

it is possible to verify that the displacement efficiency increases with L^* and decreases with D^* for a fixed value of ρ^*. Furthermore, it was observed that there is a critical value of the Reynolds number that defines the trend of the evolution of displacement efficiency in the eroded zone.

For $D^* = 1.47$, the efficiency increases with the Reynolds number, except when comparing $Re = 10.65$ and $Re = 35.62$. In this case, the largest Re, which has the smallest η^*, gives slightly less displacement efficiency. In this way, it is possible to observe that a small difference in the viscosity ratio, namely $\Delta\eta^* = 0.12$ generates a greater resistance in the flow capable of influencing the displacement efficiency.

For $D^* = 3.27$, there is a non-linear behavior about the influence of Re and η^* on displacement efficiency. It grows with the Reynolds number in the range from $Re = 4.05$ to $Re = 10.65$, while for $10.65 < Re < 35.62$ the efficiency decreases due to increased inertia and possible advection in the flow. Similar results were found by Naccache et al. (Naccache *et al.*, 2018). For $35.62 < Re < 102.57$, it is observed that for the smallest L^* there is a reduction of Φ and the inverse occurs for the largest value of L^* investigated.

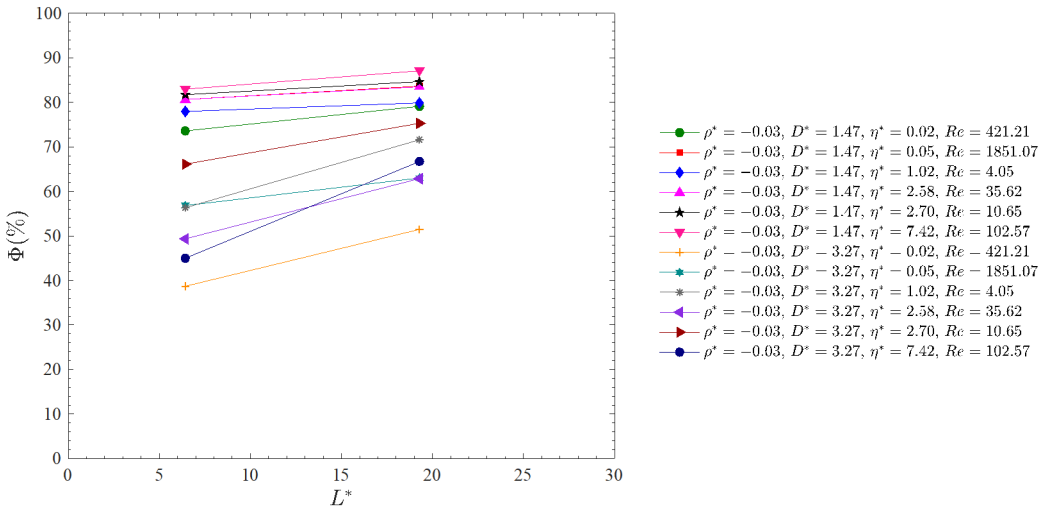

Figure 6. Displacement efficiency as a function of L^* for $\rho^* = -0.03$ and $d'^* = 0.786$.

Figures 7, 8 and 9 present the results of numerical simulations performed with $\rho^* = -0.01$ and $d'^* = 0.846$. It represents an inlet and outlet annulus length of 0.51m̀, the well diameter of 26" and the casing diameter is 22". Trends similar to those in Figure 6 were observed.

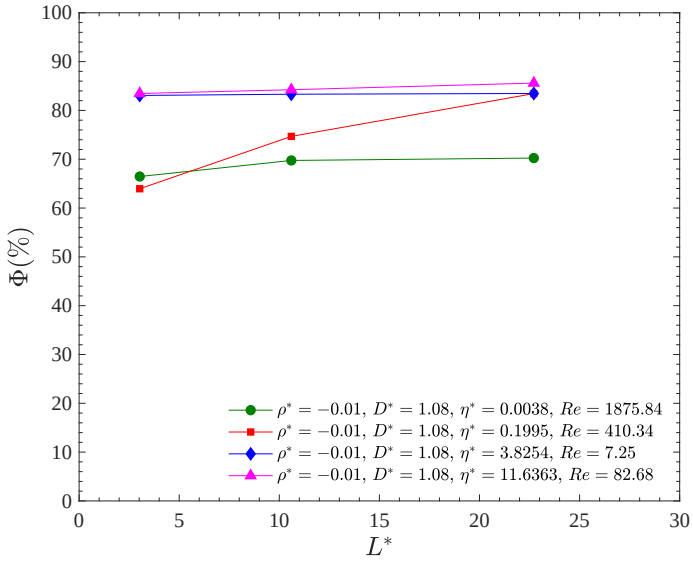

Figure 7. Displacement efficiency as a function of L^* for $\rho^* = -0.010$, $d'^* = 0.846$ and $D^* = 1.08$.

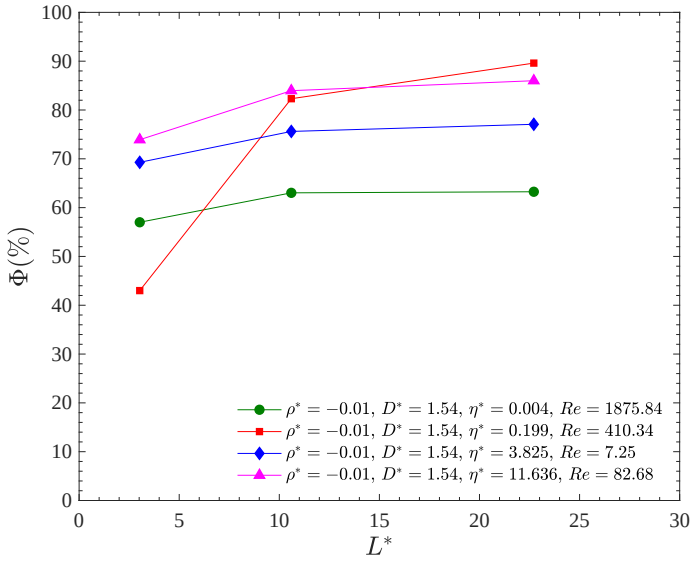

Figure 8. Displacement efficiency as a function of L^* for $\rho^* = -0.010$, $d'^* = 0.846$ and $D^* = 1.54$.

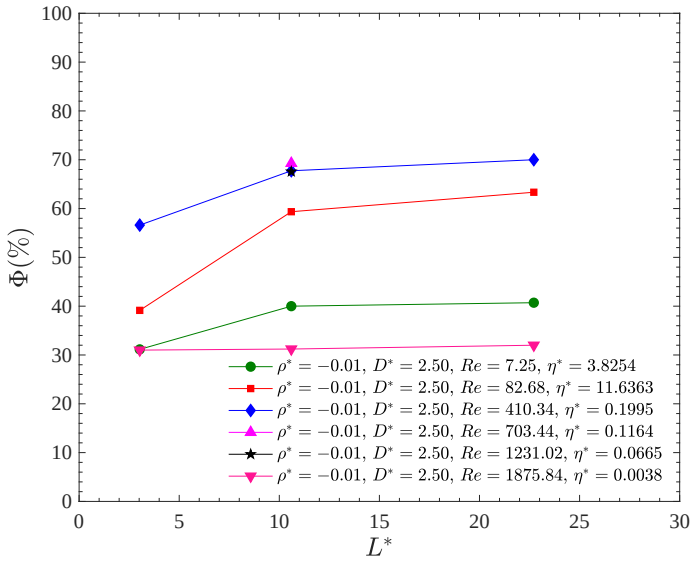

Figure 9. Displacement efficiency as a function of L^* for$\rho^* = -0.010$, $d'^* = 0.846$ and $D^* = 2.50$.

Concerning viscosity ratio, it was observed that when η^* and Re increases, the yield stress is overcome in all regions, inertia seems to become dominant, and most of fluid 1 is removed, except for a region close to the entrance. Moreover, it was also observed that the displacement efficiency is not a monotonic function of the Reynolds number.

Figure 10 presents the influence of the imposed flow rate on displacement efficiency for a fixed geometry ($D^* = 1.54$, $L^* = 22.71$, $d'^* = 0.85$) and with the same pair of fluids ($\rho^* = -0.010$). Figure 10(a) shows the volume fraction field imposing 4bpm ($\eta^* = 3.83$ and $Re = 7.25$) while Fig. 10(b) presents a flow rate of 15bpm ($\eta^* = 11.63$ and $Re = 82.68$). It was observed that Φ increases from 77 to 86% with η^* and decreases with Re.

6. CONCLUSIONS

We experimentally and numerically studied the flow of yield stress materials through annular abrupt expansions–contractions forming an axisymmetric cavity. The effect of geometry on displacement efficiency was investigated varying the enlarged region length L and diameter D. In general, it was observed that displacement efficiency increases and reaches asymptotic values as L^* increases and that Φ decreases with D^*. It was also observed that the displacement efficiency is not a monotonic function of the Reynolds number and viscosity ratio. Moreover, it strongly increases with density difference.

7. ACKNOWLEDGEMENTS

The authors are indebted to Petrobras S.A., CNPq, CAPES, ANP, FINEP, MCT and FAPERJ for the financial support to the Group of Rheology at PUC-Rio.

Figure 10. Flow rate influence on displacement efficiency: (a) 4bpm and (b) 15bpm.

8. REFERENCES

ANSYS, 2020. *ANSYS Fluent User's Guide,*. Ansys Inc., release 2020r2 edition.

Beverly, C. and Tanner, R., 1992. "Numerical analysis of three-dimensional Bingham plastic flow". *Journal of Non-Newtonian Fluid Mechanics*, Vol. 42, No. 1, pp. 85–115. ISSN 0377-0257. doi:https://doi.org/10.1016/0377-0257(92)80006-J.

Burgos, G.R. and Alexandrou, A.N., 1999. "Flow development of Herschel–Bulkley fluids in a sudden three-dimensional square expansion". *Journal of Rheology*, Vol. 43, No. 3, pp. 485–498. doi:10.1122/1.550993.

Denn, M.M. and Bonn, D., 2010. "Issues in the flow of yield-stress liquids". *Rheologica Acta*, Vol. 50, No. 4, pp. 307–315. doi:10.1007/s00397-010-0504-3.

Espinoza, P.J.T., Varges, P.R., Rodrigues, E.C., Naccache, M.F. and de Souza Mendes, P.R., 2022. "Displacement flow of yield stress materials in annular spaces of variable cross section". *Journal of Petroleum Science and Engineering*, Vol. 208, p. 109614. ISSN 0920-4105. doi:https://doi.org/10.1016/j.petrol.2021.109614.

Espinoza, P.J.T., 2020. *Deslocamento de fluidos complexos em espaços anulares irregulares*. Ph.D. thesis, Pontifícia Universidade Católica do Rio de Janeiro.

Etrati, A., Roustaei, A. and Frigaard, I., 2020. "Strategies for mud-removal from washouts during cementing of vertical surface casing". *Journal of Petroleum Science and Engineering*. doi:https://doi.org/10.1016/j.petrol.2020.107454.

Frigaard, I.A., Paso, K.G. and de Souza Mendes, P.R., 2017. "Bingham's model in the oil and gas industry". *Rheol. Acta*, Vol. 56, No. 3, pp. 259–282.

Lindner, A., Coussot, P. and Bonn, D., 2000. "Viscous fingering in a yield stress fluid". *Physical Review Letters*, Vol. 85, No. 2, pp. 314–317. doi:10.1103/physrevlett.85.314.

Moyers-Gonzalez, M.A. and Frigaard, I.A., 2008. "Kinematic instabilities in two-layer eccentric annular flows, part 2: shear-thinning and yield-stress effects". *Journal of Engineering Mathematics*, Vol. 65, No. 1, pp. 25–52. doi:10.1007/s10665-008-9260-0.

Naccache, M., Mieles Pinto, H. and Abdu, A., 2018. "Flow displacement in eroded regions inside annular ducts". *Journal of the Brazilian Society of Mechanical Sciences and Engineering*. doi:10.1007/s40430-018-1342-y.

R. Varges, P., M. Costa, C., S. Fonseca, B., F. Naccache, M. and De Souza Mendes, P.R., 2019. "Rheological Characterization of Carbopol ®. Dispersions in Water and in Water/Glycerol Solutions". *Fluids*. doi:10.3390/fluids4010003.

Roustaei, A., Gosselin, A. and Frigaard, I., 2015. "Residual drilling mud during conditioning of uneven boreholes in primary cementing. part 1: Rheology and geometry effects in non-inertial flows". *Journal of Non-Newtonian Fluid Mechanics*. doi:https://doi.org/10.1016/j.jnnfm.2014.09.019.

Soares, E.J., Naccache, M.F. and Souza Mendes, P.R., 2003. "Heat transfer to viscoplastic materials flowing axially through concentric annuli". *International Journal of Heat and Fluid Flow*, Vol. 24, No. 5, pp. 762–773. ISSN 0142-727X. doi:https://doi.org/10.1016/S0142-727X(03)00066-3.

Varges, P.R., Fonseca, B.S., de Souza Mendes, P.R., Naccache, M.F. and de Miranda, C.R., 2020. "Flow of yield stress materials through annular abrupt expansion–contractions". *Physics of Fluids*. doi:10.1063/5.0015400.

Varges, P., Rodrigues, E., Moraes, L., de Souza Mendes, P. and Naccache, M., 2022. "Flow instabilities in fluid displacement through enlarged regions in annular ducts". *Journal of Non-Newtonian Fluid Mechanics*, Vol. 305, p. 104834. ISSN 0377-0257. doi:https://doi.org/10.1016/j.jnnfm.2022.104834.

9. RESPONSIBILITY NOTICE

The authors are solely responsible for the printed material included in this paper.